LA-5662-MS

UC-34c
Reporting Date: June 1974
Issued: August 1974

Fourteen-MeV, Neutron-Induced Gamma-Ray Production Cross Sections

by

Darrell M. Drake
Edward D. Arthur
Myron G. Silbert

los alamos
scientific laboratory
of the University of California
LOS ALAMOS, NEW MEXICO 87544

UNITED STATES
ATOMIC ENERGY COMMISSION
CONTRACT W-7405-ENG. 36

Printed in the United States of America. Available from
National Technical Information Service
U.S. Department of Commerce
5285 Port Royal Road
Springfield, Virginia 22151
Price: Printed Copy $4.00 Microfiche $1.45

FOURTEEN-MEV, NEUTRON-INDUCED GAMMA-RAY PRODUCTION CROSS SECTIONS

by

Darrell M. Drake, Edward D. Arthur, and Myron G. Silbert

ABSTRACT

A pulsed 14.2-MeV neutron source and NaI(Tl) gamma-ray spectrometer were used to measure gamma-ray production cross sections for carbon, magnesium, aluminum, chromium, iron, nickel, copper, molybdenum, niobium, tantalum, platinum, ^{235}U, and ^{239}Pu.

I. INTRODUCTION

Gamma-ray production cross sections were measured for samples of carbon, magnesium, aluminum, chromium, iron, nickel, copper, molybdenum, niobium, tantalum , platinum, ^{235}U, and ^{239}Pu that were bombarded with a pulsed 14.2-MeV neutron beam obtained from the $^{2}H(t,n)^{4}He$ reaction. These cross sections are of interest for applications to the controlled thermonuclear reaction (CTR) program and to various other Laboratory programs.

II. EXPERIMENTAL ARRANGEMENT

Figure 1 shows the experimental arrangement. A chopped beam of tritons (10-ns time width at 2-mHz repetition rate) was accelerated to 2.3 MeV by the Los Alamos Scientific Laboratory (LASL) Vertical Van de Graaff. The triton beam pulses were condensed to a time width of 1 ns and directed into a deuterium gas target. Neutrons, emitted at 90° to the triton beam with a mean energy of 14.2 MeV, interacted with one of the samples placed about 100 mm from the neutron source. The energy spread of the neutrons intercepted by the samples was about ±0.5 MeV. Gamma rays produced from the bombarded samples were collimated and pulse-height analyzed by a heavily shielded NaI(Tl) crystal and photomultiplier system. An anti-Compton NaI(Tl) scintillator surrounding the center crystal was used to suppress further the background events and to improve the response functions. The pulsed neutron beam allowed time-of-flight (TOF) discrimination by sorting out the desired gamma rays from neutron-related and other background events in the crystal.

III. DATA REDUCTION

A. Background Subtraction

Figure 2 shows a relative time spectrum of NaI(Tl) pulses. Time gates were set as indicated to record pulses with differing time relationships relative to a fiducial time signal from a beam pickoff loop. Gate 1 covered the time region containing prompt gamma rays directly from the sample. Gate 2 was set to cover a time region before the neutrons from a pulse had arrived at the sample and therefore was a measure of

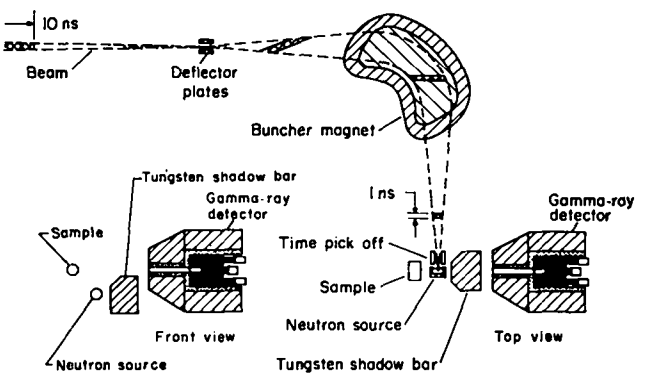

Fig. 1.
Experimental arrangement for the measurements of gamma-ray spectra. The detector and sample are about 100 mm above the plane defined by the beam path.

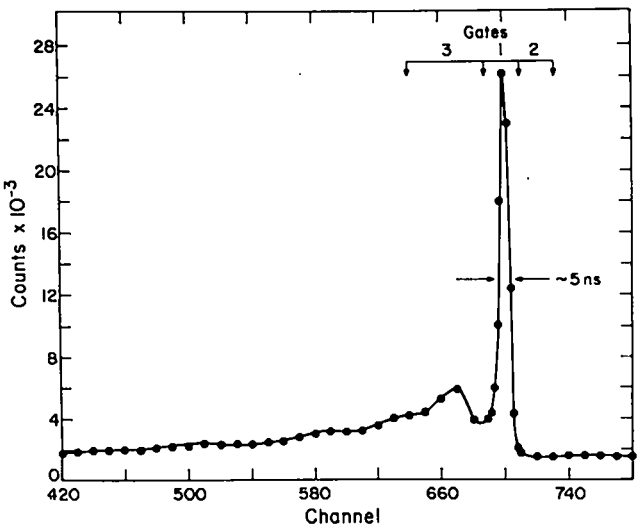

Fig. 2.
Time spectrum of pulses in the gamma-ray detector relative to the beam burst pickoff time. Gate 1 corresponds to gamma rays made in the sample due to the burst of neutrons. Gate 2 corresponds to a time-independent background. Gate 3 corresponds to fast neutron interactions in the NaI crystal.

time-independent background. Gate 3 covered times after the direct gamma rays had arrived at the scintillator and therefore was assumed to correspond to neutron-related events in the crystal that were delayed by the neutron TOF.

The first step in data reduction was to subtract the background pulse-height spectrum of Gate 2, properly normalized, from the pulse-height spectrum defined by Gate 1. Next, a separate spectrum, measured with no sample in position and the same time gates, was subtracted to obtain a net pulse-height spectrum.

The net spectra for the samples used in this experiment (except for iron) are shown in Figs. 3 through 14. Figure 15 shows the pulse-height spectrum for iron before subtracting the no-sample spectrum. This figure also shows the corresponding no-sample spectrum. The computer program NIBL converted the net pulse-height spectra to gamma-ray spectra, using knowledge of the NaI(Tl) spectrometer's response to monoenergetic gamma rays.

B. Response Functions

The response functions and efficiencies used in analyzing the experimental data were obtained by measuring the gamma-ray line shapes of calibrated

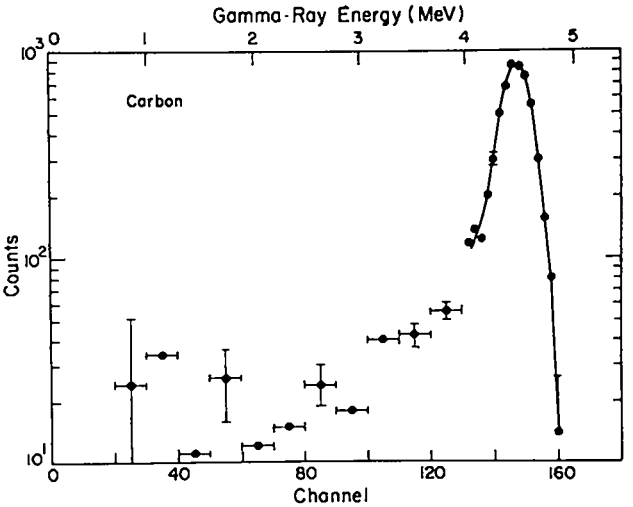

Fig. 3.
Net gamma-ray pulse-height spectrum for carbon.

sources over the 0.28- to 4.4-MeV energy range. The response functions are shown in Fig. 16 for 4.4-, 2.75-, 1.37-, and 0.66-MeV lines originating from neutron-bombarded carbon, ^{24}Na, and ^{137}Cs radioactive sources. The unfolded spectra (not corrected for efficiency) strongly resemble the net pulse-height spectra because the response functions have such a favorable peak-to-tail ratio.

The samples used in the collection of experimental data influence the shape of the gamma-ray response function; therefore, the response measurements were made so as to account for these sample-dependent effects. For example, Fig. 17 shows the gamma-ray

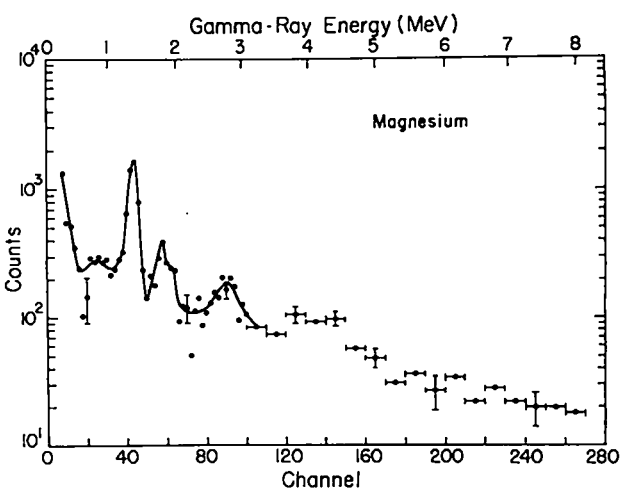

Fig. 4.
Net gamma-ray pulse-height spectrum for magnesium.

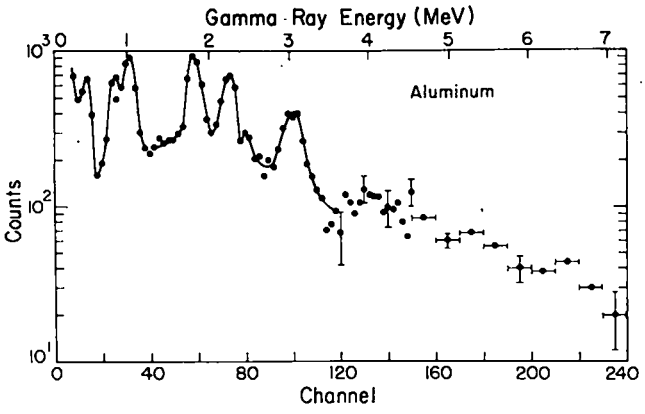

Fig. 5.
Net gamma-ray pulse-height spectrum for aluminum.

pulse-height spectrum for the 1.27-MeV gamma ray from ^{22}Na for a bare source and for the situation where a 0.32-mm-thick iron absorber was placed between the source and the detector. With the iron absorber in place, the ratio R (number of counts in the tail extending from the full energy peak to zero energy to the total number of counts in the tail plus peak) increased over the same ratio for the bare source case. The effect results from two phenomena. (1) The gamma rays were degraded in energy by scattering in the sample and were added to the number of counts occurring in the tail, and (2) the number of counts in the peak was decreased by the expected amount as a result of absorption and scattering.

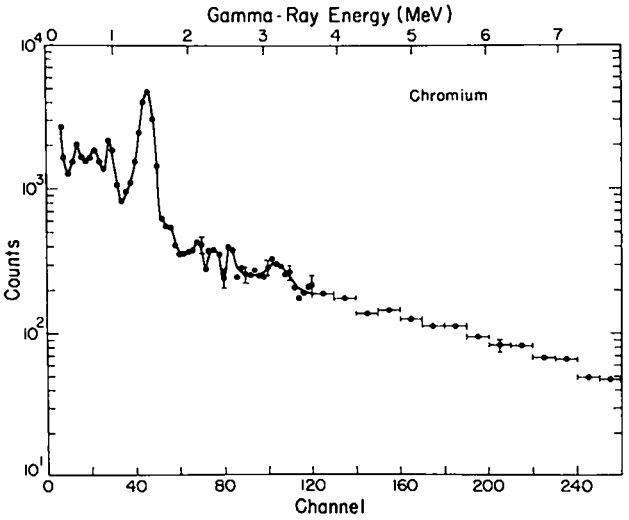

Fig. 6.
Net gamma-ray pulse-height spectrum for chromium.

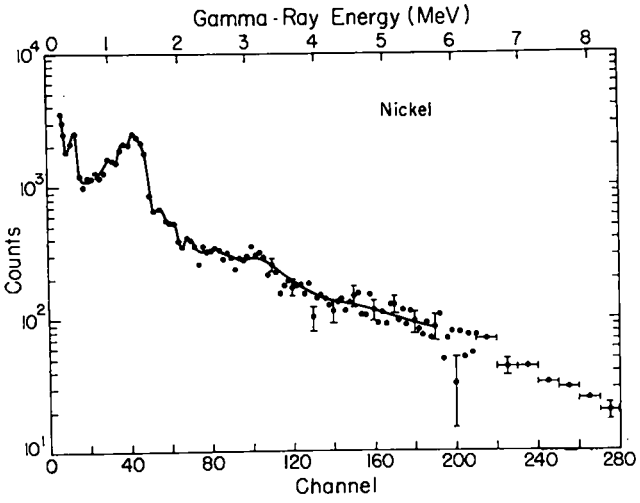

Fig. 7.
Net gamma-ray pulse-height spectrum for nickel.

To simulate the geometry of the samples actually used to obtain the experimental data, response measurements were made for situations where sources were placed inside a thin-walled iron cylinder, between two thin iron disks, as well as isolated sources. The ratio of counts in the tail divided by counts in the tail plus counts in the peak (after correction for gamma-ray absorption) was determined for these source geometries.

An estimate of the sample geometry effect was made to extend these measurements to other samples. Details of this calculation are described in

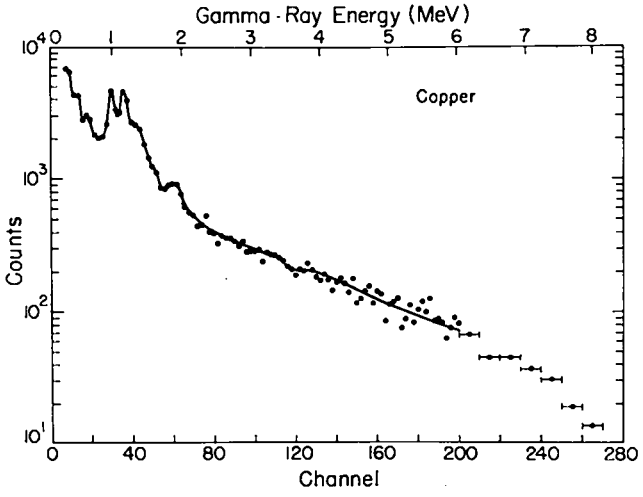

Fig. 8.
Net gamma-ray pulse-height spectrum for copper.

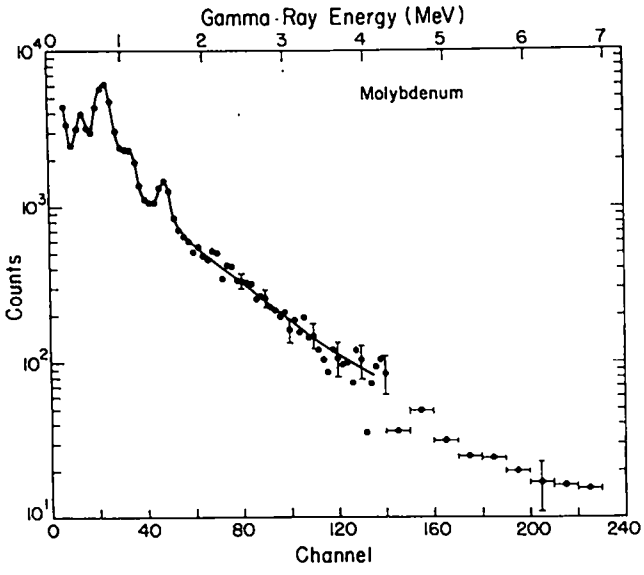

Fig. 9.
Net gamma-ray pulse-height spectrum for molybdenum.

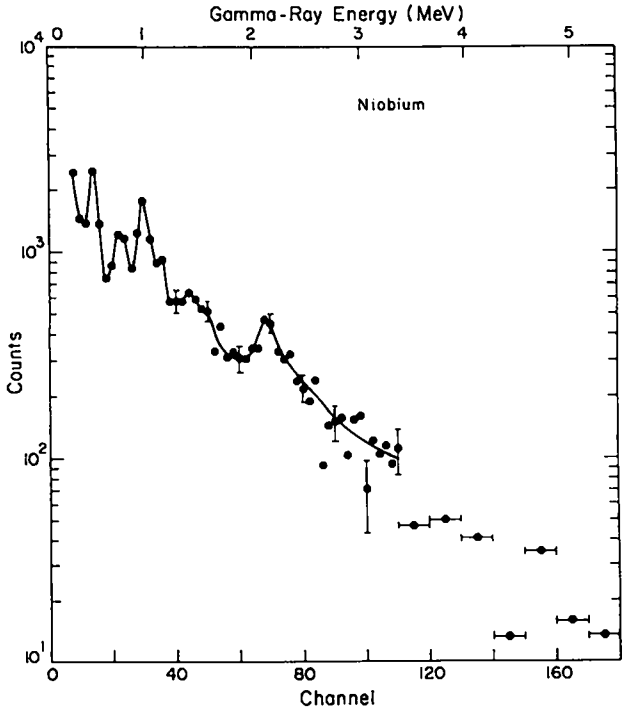

Fig.10.
Net gamma-ray pulse-height spectrum for niobium.

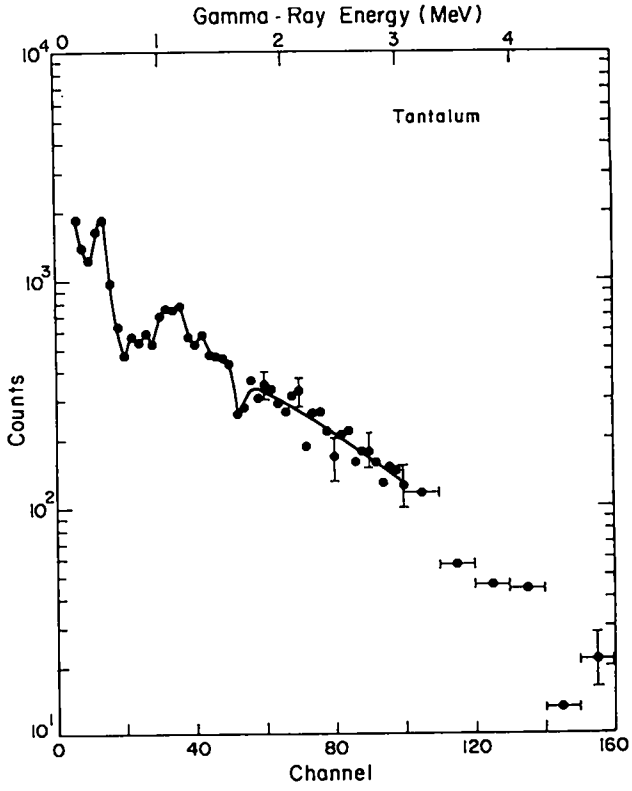

Fig. 11.
Net gamma-ray pulse-height spectrum for tantalum.

the Appendix and indicate that the ratio R for an arbitrary sample can be related to the measured ratio for the iron standard by

$$R_{sa} = R_{st} \frac{\left[1 - e^{-(n_{sa}\sigma_{sa}/2)}\right]}{\left[1 - e^{-(n_{st}\sigma_{st}/2)}\right]} .$$

Here, R_{sa} is the ratio of counts in the tail divided by total counts in the tail plus peak observed with a sample, σ_{sa} is the scattering cross section of the sample, and n_{sa} is the areal density of the sample. The equivalent quantities for the standard (here taken as iron) are R_{st}, σ_{st}, and n_{st}. By this method the ratio R was obtained for all of the samples used in the experiment.

Finally, the gamma-ray line shapes obtained from the detector were described in terms of (1) a Gaussian distribution around the peak energy with (2) a relatively flat tail extending to zero energy. The ratio R was parametrized over the 0.2- to 10-MeV gamma-ray energy range. This information, with the absolute efficiency of the detector, was incorporated into NIBL, which derived the desired photon spectra by

successively stripping NaI(Tl) response functions from the net NaI(Tl) spectra.

C. Neutron Flux Measurements

During this experiment, several separate measurements were made of the absolute neutron intensity. Two proton-recoil telescopes with different geometrical arrangements were used. Both counters used silicon and NaI(Tl) detectors in a coincidence arrangement to distinguish the recoil proton pulses from other pulses. A large resolving time (~5- to 8-μs) was used in the coincidence circuit to ensure that no proton pulses were lost due to time jitter. Further, electronic livetime (greater than 99%) was measured by connecting a 60-Hz pulser to the test input of both preamplifiers and computing the ratio of the number of these pulses that appeared in the spectra to the number of times the pulser fired.

The neutron intensity was measured as a function of the gas cell pressure and beam current over the small pressure range used in these experiments. All of the measurements agreed to within 5% with the neutron intensity calculations, which were made using appropriate cross sections for the $^{2}H(t,n)^{4}He$

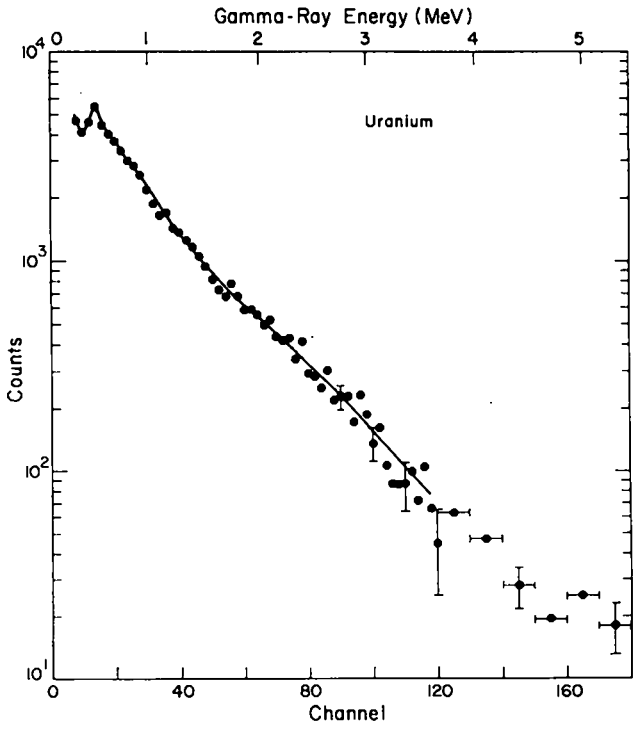

Fig. 13.
Net gamma-ray pulse-height spectrum for ^{235}U.

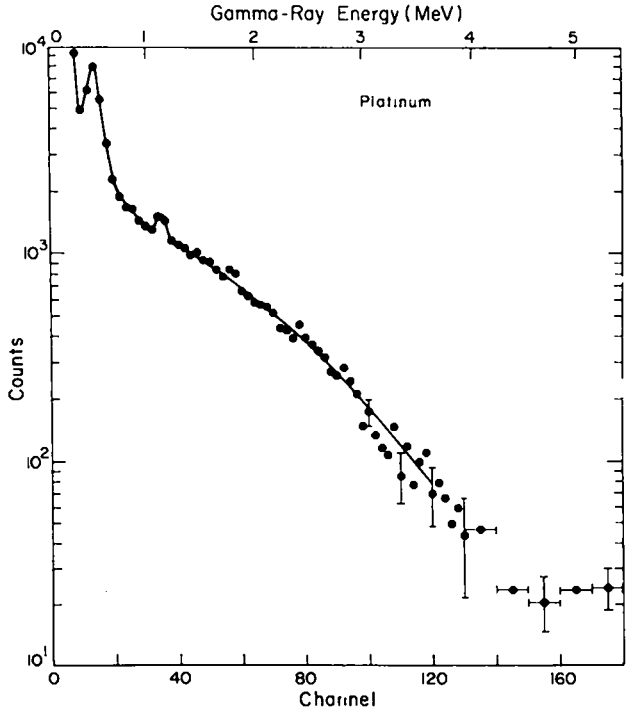

Fig. 12.
Net gamma-ray pulse-height spectrum for platinum.

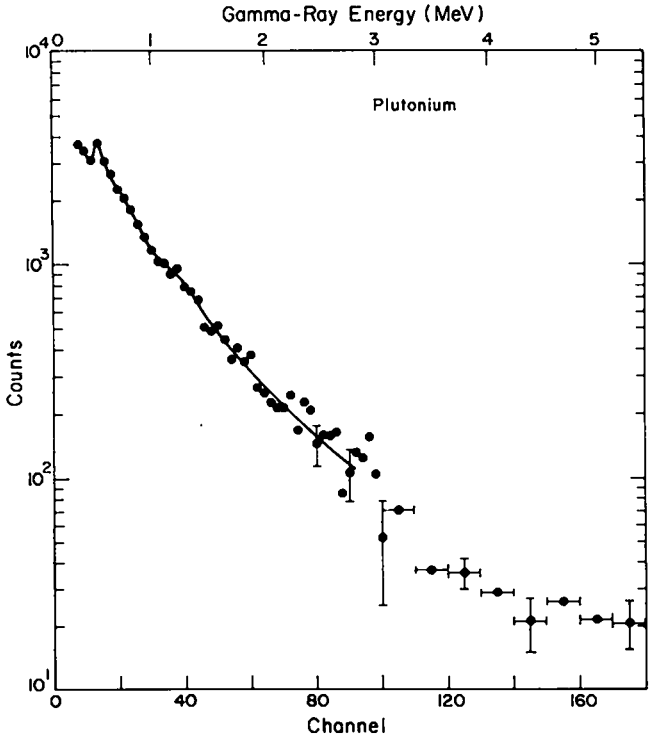

Fig. 14.
Net gamma-ray pulse-height spectrum for ^{239}Pu.

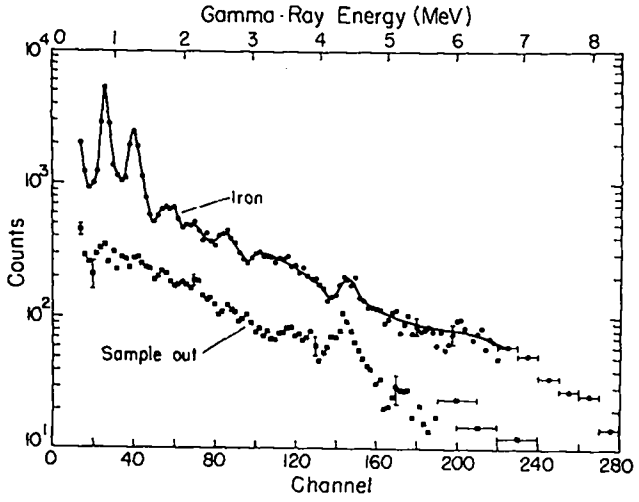

Fig. 15.
Pulse-height spectrum for iron (time-independent background was subtracted) and a corresponding no-sample pulse-height spectrum.

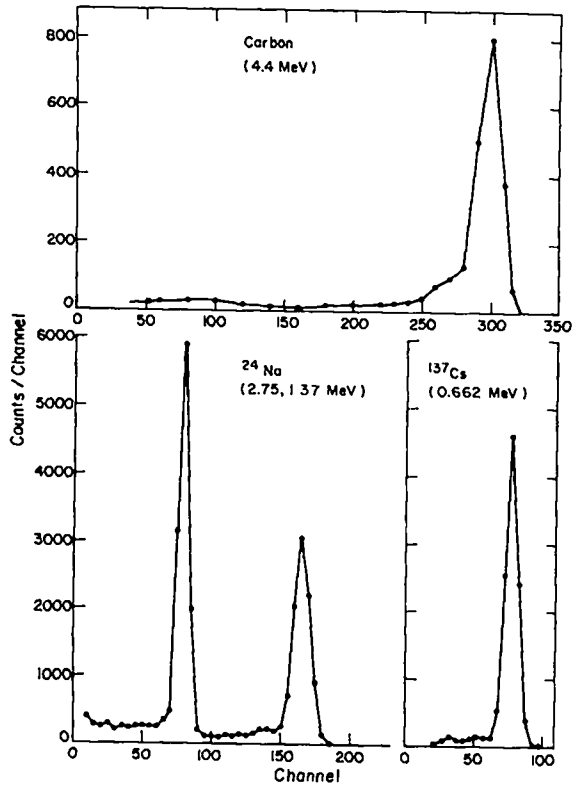

Fig. 16.
Gamma-ray pulse-height spectra for monoenergetic gamma rays. The 4.4-MeV line was obtained from neutron bombardment of carbon; the other lines were obtained from radioactive sources of ^{24}Na and ^{137}Cs.

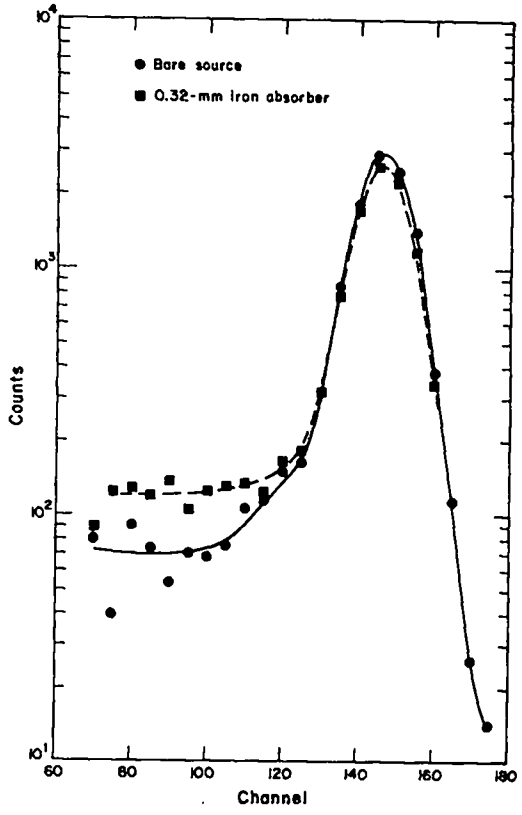

Fig. 17.
Gamma-ray pulse-height spectrum for the 1.27-MeV gamma ray from ^{22}Na with (■——■) and without (●——●) an iron absorber. This figure shows the effect of the gamma-ray production sample in modifying bare source response functions.

reaction, target pressure, and beam current. Figure 18 shows the coincident pulse-height spectra obtained for the silicon and NaI detectors, with and without the polyethylene foil. Telescope efficiency was calculated using the geometrical corrections described by Hansen et al.[1] and the H(n,p)n cross sections of Hopkins and Breit.[2]

D. Multiple Scattering

The multiple scattering effect of neutrons in the samples was estimated using the code MCN.[3] For the nonfissionable samples, the correction was applied to the data as a function of gamma-ray energy. In general, a nonelastic collision in any of the samples reduces the neutron energy to such an extent that a second nonelastic collision cannot produce high-energy gamma rays. Therefore, the full magnitude of the correction indicated by MCN was applied to the

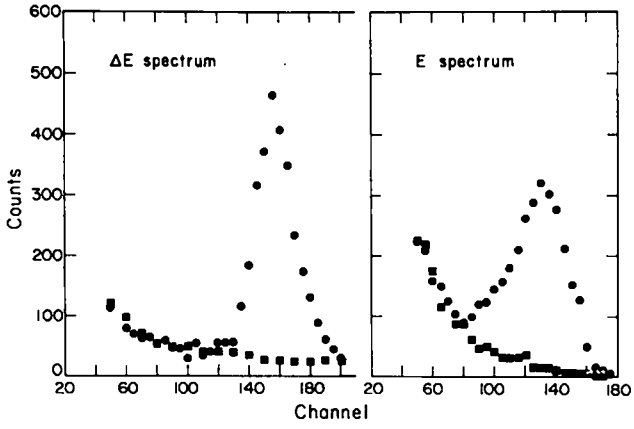

Fig. 18.
Pulse-height spectra for the proton recoil telescope for both ΔE (silicon) and E[NaI(Tl)] detectors. Squares represent background counts with the polyethylene radiator removed.

low-energy (0.5-MeV) part of the gamma-ray spectrum and was decreased linearly to zero at 8 MeV. This rather arbitrary procedure introduces only small uncertainties because the multiple scattering effect is only about 4% or less.

For the fissionable elements, the correction was applied to the entire spectrum because most of the gamma rays are associated with fission fragments and the spectrum shape is not altered by multiple scattering.

E. Cross-Section Calculations

Differential cross sections were calculated for gamma-ray production as a function of gamma-ray energy by

$$\sigma(E_\gamma,\theta) = \frac{N_\gamma \times d^2}{F \times \epsilon(E_\gamma) \times N}, \qquad (1)$$

where N_γ is the number of gamma rays in an energy interval, d^2 is the harmonic mean of the square of the distance from the neutron source to the sample, F is the time-integrated neutron flux, $\epsilon(E_\gamma)$ is the efficiency of the gamma-ray spectrometer for gamma-ray energy E_γ, and N is the number of sample atoms. Corrections were made for multiple scattering of neutrons in the sample ($\leq$5%), deadtime (~5-8%), and gamma-ray attenuation in the sample.

IV. ESTIMATE OF ERRORS

Uncertainties in the gamma-ray detector efficiency were estimated to be ±3% from 0.5 to 3 MeV, increasing to ±12% at 8 MeV.

Neutron flux measurements were very consistent throughout the experiment, and the uncertainty in the flux was taken to be ±7%.

Errors introduced by the unfolding program, including the use of imperfect response functions, were taken to be ±5%.

Multiple scattering corrections were typically less than 5%. The uncertainty assigned to this correction was taken to be half the value indicated by the MCN code.

Precision of the measurement of the sample position relative to the neutron source was about ±1 mm. This introduced an uncertainty of about ±3% in cross sections.

Statistical standard deviations were added in quadrature to the above uncertainties and are included in the cross-section tables.

V. RESULTS

Cross sections for gamma-ray production on all samples included in this report except carbon are listed in Table I. Table II lists cross sections for those gamma rays that can be analyzed as individual lines. In Table I cross sections are listed as millibarns per steradian in 100-keV intervals from 300 to 4000 keV, and in 500-keV intervals above 4000 keV. The energy-weighted integral cross sections, $\int E_\gamma \sigma(E_\gamma)\, dE_\gamma$, for ^{235}U and ^{239}Pu from 0.3 to 9 MeV are 23.5 ± 2.8 and 25.4 ± 3.0 MeV-b, respectively.

Table II lists cross sections for separable gamma rays for the lighter elements (carbon through iron). Some of these cross sections might include some nearby gamma rays. For example, the 0.84-MeV gamma-ray cross section listed for iron probably contains some of the 0.93-MeV gamma rays from the $^{56}Fe(n,2n)^{55}Fe$ reaction. There are some peaks in the spectra for heavier elements, but no attempt was made to analyze them as single gamma rays.

TABLE I

DIFFERENTIAL GAMMA-RAY PRODUCTION CROSS SECTIONS AS A FUNCTION OF GAMMA-RAY ENERGY

Element →	MAGNESIUM				ALUMINUM		CHROMIUM		IRON			
Angle →	90°		128°		128°		120°		90°		120°	
Energy Interval (MeV)	Cross Section (mb/sr)	Est Uncertainty (mb/sr)	Cross Section (mb/sr)	Est Uncertainty (mb/sr)	Cross Section (mb/sr)	Est Uncertainty (mb/sr)	Cross Section (mb/sr)	Est Uncertainty (mb/sr)	Cross Section (mb/sr)	Est Uncertainty (mb/sr)	Cross Section (mb/sr)	Est Uncertainty (mb/sr)
0.3 - 0.4	5.1	0.6	7.2	1.0	2.3	0.6	6.5	0.9	6.2	0.6	8.1	1.3
0.4 - 0.5	2.8	0.4	3.7	0.8	3.2	0.6	9.8	1.1	12.1	1.3	10.2	1.2
0.5 - 0.6	1.7	0.3	1.8	0.5	0.61	0.36	9.1	1.0	8.3	0.9	4.2	0.3
0.6 - 0.7	0.56	0.21	0.36	0.46	0.0	0.35	9.8	1.1	5.0	0.5	1.8	0.7
0.7 - 0.8	1.5	0.2	2.0	0.5	3.2	0.5	10.4	1.1	15.0	1.5	15.7	2.0
0.8 - 0.9	2.7	0.3	2.3	0.5	3.4	0.5	10.5	1.1	34.5	3.5	43.4	4.6
0.9 - 1.0	2.0	0.3	2.0	0.5	6.0	0.7	12.2	1.3	11.8	1.2	12.8	1.5
1.0 - 1.1	1.9	0.3	1.5	0.5	4.1	0.5	5.0	0.6	6.5	0.7	6.9	0.8
1.1 - 1.2	2.8	0.3	2.3	0.5	1.2	0.3	6.1	0.6	9.7	1.1	11.0	1.4
1.2 - 1.3	5.5	0.6	6.2	0.8	1.5	0.3	11.6	1.2	18.6	1.8	23.3	2.4
1.3 - 1.4	16.5	1.7	17.9	1.9	1.3	0.3	29.5	3.0	10.0	1.0	13.3	1.4
1.4 - 1.5	8.3	0.9	8.5	1.0	1.2	0.3	33.7	3.4	4.1	0.4	4.9	0.6
1.5 - 1.6	2.2	0.3	1.3	0.4	1.4	0.3	12.4	1.3	2.7	0.3	3.0	0.5
1.6 - 1.7	2.3	0.3	1.8	0.4	3.1	0.4	2.8	0.4	3.6	0.4	4.0	0.5
1.7 - 1.8	3.6	0.4	3.1	0.5	7.1	0.8	3.4	0.4	4.5	0.5	5.4	0.6
1.8 - 1.9	3.6	0.4	3.4	0.5	6.5	0.7	2.2	0.3	4.3	0.5	4.7	0.6
1.9 - 2.0	2.0	0.2	2.5	0.4	2.9	0.4	2.3	0.3	3.1	0.3	3.6	0.4
2.0 - 2.1	1.1	0.2	1.1	0.3	2.4	0.3	2.6	0.4	2.9	0.3	3.2	0.4
2.1 - 2.2	1.0	0.2	0.75	0.27	4.7	0.5	2.2	0.3	3.0	0.3	3.2	0.4
2.2 - 2.3	0.97	0.15	0.49	0.25	6.0	0.7	2.3	0.3	2.3	0.3	2.4	0.3
2.3 - 2.4	0.98	0.14	1.1	0.3	3.6	0.4	2.3	0.3	2.2	0.3	2.5	0.4
2.4 - 2.5	1.3	0.2	0.93	0.24	2.3	0.3	1.7	0.3	2.7	0.3	2.7	0.4
2.5 - 2.6	1.4	0.2	1.4	0.3	1.7	0.3	1.8	0.2	3.2	0.4	3.6	0.5
2.6 - 2.7	1.7	0.2	1.8	0.3	1.3	0.2	1.6	0.2	2.7	0.3	3.2	0.4
2.7 - 2.8	1.9	0.2	2.3	0.3	1.4	0.2	1.7	0.2	2.1	0.2	2.4	0.3
2.8 - 2.9	1.7	0.2	2.0	0.3	1.9	0.3	1.6	0.2	1.9	0.2	2.0	0.3
2.9 - 3.0	1.1	0.1	1.2	0.3	3.7	0.4	1.7	0.2	1.9	0.2	2.1	0.3
3.0 - 3.1	0.97	0.14	1.0	0.2	3.9	0.5	2.3	0.3	1.8	0.2	2.0	0.3
3.1 - 3.2	0.79	0.12	1.1	0.2	2.4	0.3	2.3	0.3	2.0	0.2	2.2	0.3
3.2 - 3.3	0.67	0.11	0.67	0.21	1.4	0.2	2.3	0.3	2.0	0.2	2.5	0.3
3.3 - 3.4	0.54	0.10	0.64	0.20	0.96	0.18	1.8	0.3	1.9	0.2	2.3	0.3
3.4 - 3.5	0.75	0.12	1.1	0.2	0.62	0.16	1.3	0.2	1.9	0.2	2.2	0.3
3.5 - 3.6	0.69	0.11	0.5	0.21	0.53	0.16	1.6	0.2	1.9	0.2	2.3	0.3
3.6 - 3.7	0.92	0.13	0.95	0.22	0.78	0.17	1.8	0.2	1.8	0.2	2.2	0.3
3.7 - 3.8	1.34	0.2	1.0	0.2	0.90	0.18	1.5	0.2	1.7	0.2	2.0	0.3
3.8 - 3.9	1.5	0.2	1.5	0.3	0.88	0.18	1.7	0.2	1.4	0.2	1.7	0.3
3.9 - 4.0	1.4	0.2	1.4	0.3	1.2	0.2	1.4	0.2	1.4	0.2	1.7	0.3
4.0 - 4.5	1.3	0.27	1.3	0.27	0.94	0.20	1.4	0.2	1.2	0.2	1.4	0.2
4.5 - 5.0	0.71	0.23	0.71	0.23	0.90	0.20	1.4	0.2	1.0	0.2	1.2	0.2
5.0 - 5.5	0.51	0.21	0.51	0.21	0.75	0.19	1.2	0.2	0.99	0.14	1.2	0.2
5.5 - 6.0	0.56	0.21	0.56	0.21	0.73	0.19	1.3	0.2	0.99	0.15	1.1	0.2
6.0 - 6.5	0.56	0.24	0.56	0.24	0.56	0.21	1.0	0.2	0.98	0.17	1.2	0.2
6.5 - 7.0	0.50	0.25	0.50	0.25	0.49	0.24	0.87	0.24	0.98	0.18	1.1	0.2
7.0 - 7.5	0.59	0.24	0.59	0.24	0.56	0.23	0.94	0.25	0.88	0.16	1.0	0.2
7.5 - 8.0	0.64	0.22	0.64	0.27	0.59	0.16	0.91	0.18	0.79	0.15	0.90	0.17
8.0 - 8.5	0.41	0.13	0.41	0.13	0.32	0.11	0.91	0.18	0.69	0.13	0.79	0.18
8.5 - 9.0	0.61	0.14	0.61	0.14	0.45	0.13	0.71	0.16	0.60	0.12	0.64	0.14

TABLE I (cont)

Element →	NICKEL		COPPER		MOLYBDENUM				NIOBIUM	
Angle →	120°		120°		90°		120°		120°	
Energy Interval (MeV)	Cross Section (mb/sr)	Est Uncertainty (mb/sr)	Cross Section (mb/sr)	Est Uncertainty (mb/sr)	Cross Section (mb/sr)	Est Uncertainty (mb/sr)	Cross Section (mb/sr)	Est Uncertainty (mb/sr)	Cross Section (mb/sr)	Est Uncertainty (mb/sr)
0.3 - 0.4	12.1	1.3	22.0	2.4	---	---	22.1	2.5	29.4	3.2
0.4 - 0.5	13.2	1.4	15.8	1.7	---	---	27.6	3.6	30.5	3.3
0.5 - 0.6	3.7	0.5	10.1	1.1	20.3	2.1	24.5	2.9	17.6	1.9
0.6 - 0.7	2.5	0.4	10.1	1.1	29.4	3.0	40.6	4.5	12.2	1.5
0.7 - 0.8	5.0	0.5	6.7	0.7	52.5	5.3	63.4	6.7	16.7	1.8
0.8 - 0.9	4.6	0.5	10.6	1.0	42.9	4.3	46.3	4.8	14.9	1.7
0.9 - 1.0	8.2	0.8	21.0	2.1	22.6	2.3	25.5	2.7	25.2	2.6
1.0 - 1.1	9.1	0.9	16.8	1.7	20.7	2.1	23.8	2.6	14.4	1.6
1.1 - 1.2	12.5	1.2	23.9	2.4	16.6	1.7	18.6	2.0	11.6	1.3
1.2 - 1.3	15.4	1.5	15.8	1.6	11.3	1.2	12.2	1.3	7.9	1.0
1.3 - 1.4	18.8	1.9	13.3	1.4	10.5	1.1	11.6	1.3	9.7	1.2
1.4 - 1.5	16.1	1.6	9.9	1.0	13.3	1.3	15.4	1.7	9.4	1.1
1.5 - 1.6	7.5	0.8	7.3	0.8	14.1	1.4	14.7	1.6	8.1	1.0
1.6 - 1.7	4.5	0.4	5.9	0.7	9.8	1.0	9.7	1.1	7.2	0.9
1.7 - 1.8	4.6	0.5	5.0	0.5	7.7	0.8	7.4	0.8	4.4	0.7
1.8 - 1.9	4.2	0.5	5.6	0.6	6.3	0.7	6.4	0.7	6.0	0.8
1.9 - 2.0	2.9	0.3	4.5	0.5	5.9	0.6	6.1	0.7	6.2	0.8
2.0 - 2.1	2.4	0.3	3.4	0.4	5.5	0.6	5.5	0.7	7.3	0.9
2.1 - 2.2	2.4	0.3	3.1	0.4	4.8	0.5	4.9	0.6	7.3	0.9
2.2 - 2.3	2.1	0.2	2.5	0.3	4.3	0.5	4.4	0.6	6.2	0.8
2.3 - 2.4	2.2	0.2	2.5	0.3	3.9	0.4	4.2	0.5	5.0	0.6
2.4 - 2.5	2.2	0.3	2.2	0.3	3.8	0.4	3.7	0.5	3.5	0.5
2.5 - 2.6	2.1	0.2	2.1	0.3	3.2	0.3	3.3	0.4	3.2	0.5
2.6 - 2.7	2.3	0.3	1.9	0.2	3.0	0.3	3.0	0.4	2.2	0.4
2.7 - 2.8	2.2	0.3	1.8	0.2	2.8	0.3	3.0	0.4	3.0	0.5
2.8 - 2.9	2.3	0.3	1.9	0.2	2.7	0.3	2.6	0.4	2.2	0.4
2.9 - 3.0	2.4	0.3	1.7	0.2	2.2	0.2	2.3	0.3	2.4	0.4
3.0 - 3.1	2.5	0.3	1.7	0.2	2.0	0.2	2.3	0.3	1.6	0.4
3.1 - 3.2	2.3	0.3	1.6	0.2	2.0	0.2	1.9	0.3	1.3	0.4
3.2 - 3.3	2.1	0.2	1.6	0.2	1.8	0.2	2.0	0.3	1.7	0.4
3.3 - 3.4	1.9	0.2	1.6	0.2	1.7	0.2	1.7	0.3	1.5	0.4
3.4 - 3.5	1.5	0.2	1.5	0.2	1.6	0.2	1.4	0.3	0.45	0.31
3.5 - 3.6	1.4	0.2	1.3	0.2	1.4	0.2	1.4	0.3	1.1	0.3
3.6 - 3.7	1.4	0.2	1.4	0.2	1.3	0.2	1.3	0.3	1.2	0.3
3.7 - 3.8	1.3	0.2	1.3	0.2	1.3	0.2	1.0	0.2	0.68	0.33
3.8 - 3.9	1.3	0.2	1.3	0.2	1.2	0.2	1.2	0.2	1.3	0.3
3.9 - 4.0	1.1	0.2	1.1	0.2	1.1	0.1	1.0	0.2	0.86	0.32
4.0 - 4.5	1.2	0.2	1.2	0.2	0.95	0.14	0.83	0.24	0.56	0.33
4.5 - 5.0	1.1	0.2	0.95	0.17	0.69	0.11	0.66	0.23	0.65	0.28
5.0 - 5.5	1.1	0.2	0.81	0.15	0.51	0.10	0.52	0.24	0.29	0.30
5.5 - 6.0	0.96	0.17	0.78	0.15	0.45	0.09	0.46	0.29	0.35	0.30
6.0 - 6.5	0.92	0.18	0.64	0.15	0.39	0.09	0.38	0.28	0.33	0.32
6.5 - 7.0	0.81	0.18	0.59	0.15	0.26	0.09	0.33	0.25	0.30	0.38
7.0 - 7.5	0.77	0.16	0.40	0.11	0.23	0.07	0.26	0.14	0.30	0.31
7.5 - 8.0	0.67	0.13	0.29	0.07	0.15	0.05	0.17	0.11	0.12	0.14
8.0 - 8.5	0.54	0.13	0.15	0.05	0.09	0.03	0.14	0.08	0.14	0.14
8.5 - 9.0	0.36	0.08	0.13	0.05	0.08	0.03	0.13	0.08	0.13	0.12

TABLE I (cont)

Element →	TANTALUM		PLATINUM		URANIUM		PLUTONIUM	
Angle →	120°		122°		120°		120°	
Energy Interval (MeV)	Cross Section (mb/sr)	Est Uncertainty (mb/sr)	Cross Section (mb/sr)	Est Uncertainty (mb/sr)	Cross Section (mb/sr)	Est Uncertainty (mb/sr)	Cross Section (mb/sr)	Est Uncertainty (mb/sr)
0.3 - 0.4	63.4	7.4	128	13	201	20	281	29
0.4 - 0.5	71.4	7.7	152	15	217	22	262	27
0.5 - 0.6	31.0	3.7	88.5	8.9	161	17	202	21
0.6 - 0.7	16.6	2.4	35.6	3.7	130	13	154	15
0.7 - 0.8	15.9	2.3	22.4	2.4	111	11	126	13
0.8 - 0.9	17.3	2.4	20.0	2.1	93	10	102	11
0.9 - 1.0	19.4	2.5	17.6	1.9	78	7.8	81	9.6
1.0 - 1.1	23.3	2.8	20.3	2.2	63	6.4	70	8.3
1.1 - 1.2	23.1	2.8	19.8	2.1	60	6.0	65	8.1
1.2 - 1.3	16.6	2.2	16.7	1.8	55	5.5	58	7.3
1.3 - 1.4	19.0	2.4	16.8	1.8	48	4.8	48	6.1
1.4 - 1.5	16.9	2.2	16.9	1.8	40	4.1	40	4.9
1.5 - 1.6	13.9	1.9	16.9	1.8	37	3.7	36	4.5
1.6 - 1.7	13.4	1.8	16.2	1.7	34	3.3	31	4.2
1.7 - 1.8	12.0	1.7	16.2	1.7	32	3.4	29	3.8
1.8 - 1.9	12.4	1.7	13.8	1.5	28	2.8	24	3.1
1.9 - 2.0	11.5	1.5	11.3	1.2	25	2.6	21	2.7
2.0 - 2.1	10.6	1.4	10.7	1.2	21	2.2	20	2.8
2.1 - 2.2	11.2	1.5	8.8	1.0	19	2.1	19	2.6
2.2 - 2.3	9.6	1.3	8.3	0.9	18	2.0	15	2.2
2.3 - 2.4	8.9	1.2	7.9	0.9	15	1.7	14	2.1
2.4 - 2.5	7.8	1.1	7.4	0.8	14	1.5	12	2.0
2.5 - 2.6	6.7	1.0	6.5	0.7	13	1.3	12	2.0
2.6 - 2.7	6.4	1.0	6.4	0.7	12	1.3	10	1.8
2.7 - 2.8	6.8	1.0	5.4	0.6	9.9	1.1	9.5	1.7
2.8 - 2.9	5.8	0.9	5.3	0.6	9.2	1.1	9.7	1.8
2.9 - 3.0	5.2	0.9	3.7	0.5	8.6	1.0	8.0	1.6
3.0 - 3.1	4.7	0.9	3.1	0.5	6.2	0.9	5.7	1.4
3.1 - 3.2	3.4	0.8	2.6	0.4	5.8	0.8	4.7	1.4
3.2 - 3.3	4.6	0.9	3.1	0.4	5.7	0.8	8.2	1.6
3.3 - 3.4	4.1	0.8	2.3	0.4	5.3	0.8	4.5	1.3
3.4 - 3.5	2.2	0.7	1.8	0.3	4.7	0.7	4.5	1.4
3.5 - 3.6	2.6	0.8	1.9	0.3	3.7	0.7	2.3	1.3
3.6 - 3.7	2.3	0.7	1.4	0.3	3.6	0.6	4.3	1.3
3.7 - 3.8	1.2	0.7	1.9	0.4	4.0	0.7	2.3	1.3
3.8 - 3.9	3.0	0.7	1.3	0.3	4.0	0.7	3.4	1.3
3.9 - 4.0	1.8	0.7	1.5	0.3	2.9	0.7	3.6	1.3
4.0 - 4.5	1.2	0.7	0.66	0.29	2.6	0.6	1.7	1.2
4.5 - 5.0	0.77	0.61	0.71	0.26	1.8	0.6	1.4	1.0
5.0 - 5.5	0.40	0.63	0.56	0.27	1.2	0.6	1.4	1.0
5.5 - 6.0	0.60	0.64	0.14	0.27	0.7	0.6	0.6	0.6
6.0 - 6.5	0.59	0.77	0.30	0.30	0.9	0.6	0.8	0.7
6.5 - 7.0	0.84	0.93	0.35	0.37	0.7	0.7	0.9	0.8
7.0 - 7.5	0.37	0.60	0.17	0.19	0.6	0.4	0.8	0.4
7.5 - 8.0	0.19	0.35	0.19	0.15	0.3	0.2	0.5	0.3
8.0 - 8.5	0.27	0.22	0.09	0.08				
8.5 - 9.0	0.30	0.24	0.08	0.07				

TABLE II

DIFFERENTIAL GAMMA-RAY PRODUCTION CROSS SECTIONS FOR PROMINENT GAMMA RAYS

Element	Gamma-Ray Energy (MeV)	Angle	Cross Section (mb/sr)
Carbon	4.4	45	21.3 ± 2.8
		64	15.0 ± 2.0
		90	11.6 ± 1.5
		125	16.1 ± 2.1
Magnesium	1.37	122	30.3 ± 3.3
		90	27.2 ± 3.0
	1.81	122	8.3 ± 1.2
		90	8.2 ± 1.2
	2.8	122	4.2 ± 0.7
		90	6.2 ± 1.0
Aluminum	0.84	122	5.4 ± 1.1
	1.01	122	10.6 ± 2.1
	1.8	122	16.7 ± 2.5
	2.2	122	13.5 ± 2.0
	3.0	122	8.4 ± 1.3
Chromium	1.33 + 1.44	123	76.7 ± 9.2
Iron	0.845	122	65.6 ± 7.0
		90	53.2 ± 5.6
	1.24	122	34.0 ± 4.1
		90	27.8 ± 3.3

APPENDIX

MODIFICATION OF RESPONSE FUNCTIONS DUE TO PHOTON SCATTERING

Neutron-induced gamma-ray production cross-section measurements usually involve unfolding or stripping of complex pulse-height spectra. Response functions used in the unfolding process are obtained from monoenergetic gamma-ray sources and consist primarily of a Gaussian full-energy peak and a relatively flat tail due to Compton collisions in the detector.

This Appendix shows that for samples of moderate size, this tail can be significantly larger than that measured with the usual gamma-ray sources.

For simplicity, the sample is taken to be a cube with sides t in length and n atoms/cm^3, G_o monoenergetic gamma rays are produced uniformly through the sample, σ_s is the gamma-ray scattering cross section, and the detector area is ΔA and is located a distance R from the sample. Also, $n\sigma t$ is taken to be small.

Assuming that (1) $(1-\Delta A/4\pi R^2) \cong 1$, (2) efficiency for scattered gamma rays is the same as the direct gamma rays, and (3) absorption cross section for scattered gamma rays is the same as for direct gamma rays, the ratio of scattered gamma-ray counts to counts from direct gamma rays is (errors caused by assumptions 2 and 3 tend to cancel)

$$\left(1 - e^{-n\sigma_s t/2}\right) .$$

For most samples, this is a modest increase in counts (~13% for a 6.4-mm-thick sample of iron and 1.27-MeV gamma rays), but for detectors whose bare source response functions have small tails compared

to full-energy peaks, the relative magnitude of the tail can be increased significantly (Fig. 3 shows an increase of about 70%).

In complex gamma-ray spectra that have been unfolded with bare source response functions, this effect would appear to be an extra continuum of gamma rays.

REFERENCES

1. G. Hansen, R. K. Smith, Los Alamos Scientific Laboratory, and G. G. Simons, University of Wyoming, personal communication, May 1974.

2. J. C. Hopkins and G. Breit, "The $^{1}H(n,n)^{1}H$ Scattering Observables Required for High-Precision Fast-Neutron Measurements," Nucl. Data Tables **A9**, 137 (1971).

3. E. D. Cashwell, J. R. Neergaard, W. M. Taylor, and G. D. Turner, "MCN: A Neutron Monte Carlo Code," Los Alamos Scientific Laboratory report LA-4751 (January 1972).